Electroanalytical Performance of Nitrogen-Containing Tetrahedral Amorphous Carbon Thin-Film Electrodes

ARTICLE *in* ANALYTICAL CHEMISTRY · JUNE 2012

Impact Factor: 5.64 · DOI: 10.1021/ac301124r · Source: PubMed

4 AUTHORS, INCLUDING:

Greg M Swain
Michigan State University
177 PUBLICATIONS **5,588** CITATIONS

analytical chemistry

Article

pubs.acs.org/ac

Electroanalytical Performance of Nitrogen-Containing Tetrahedral Amorphous Carbon Thin-Film Electrodes

Xingyi Yang,[†] Lars Haubold,[‡] Gabriel DeVivo,[†] and Greg M. Swain*[,†]

[†]Department of Chemistry and [‡]The Fraunhofer Center for Coatings and Laser Applications Michigan State University East Lansing, Michigan 48824-1322, United States

Supporting Information

ABSTRACT: Tetrahedral amorphous carbon (ta-C) consists of a mixture of sp^3- and sp^2-bonded carbon ranging from 60 to 40% (sp^3/sp^3+sp^2) depending on the deposition conditions. The physical, chemical, and electrochemical properties depend on the sp^2/sp^3 bonding ratio as well as the presence of incorporated impurities, such as hydrogen or nitrogen. The ability to grow ta-C at lower temperatures (25−100 °C) on a wider variety of substrates as compared to CVD diamond is an advantage of this material. Herein, we report on the structural and electrochemical properties of nitrogen-incorporated ta-C thin films (ta-C:N). The incorporation of nitrogen into the films decreases the electrical resistivity from 613 ± 60 (0 sccm N_2) to 1.10 ± 0.07 Ω-cm (50 sccm N_2), presumably by increasing the sp^2-bonded carbon content and the connectedness of these domains. Similar to boron-doped diamond, these materials are characterized by a low background voltammetric current, a wide working potential window (∼ 3 V), and relatively rapid electron-transfer kinetics for aqueous redox systems, including $Fe(CN)_6^{-3/-4}$ and $Ru(NH_3)_6^{+3/+2}$, without conventional pretreatment. Additionally, there is weak molecular adsorption of polar molecules (methylene blue) on the ta-C surface. Overall, the properties of the ta-C and ta-C:N electrodes are such that they could be excellent new choices for electroanalytical measurements.

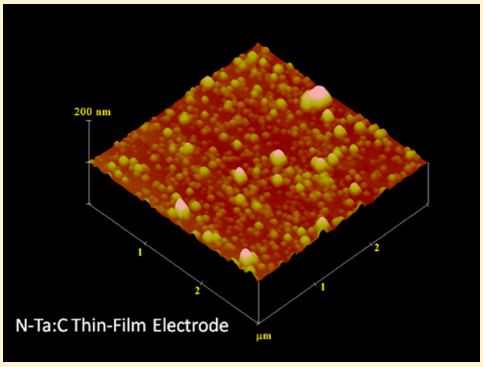

The sp^2 carbon electrodes have been used extensively over the years in electroanalytical measurements. Much is known about the structure−function relationships of these electrodes.[1−3] Boron-doped diamond (BDD) is an sp^3-bonded carbon material with some superb properties for electroanalytical measurements.[4−9] Even though BDD has been successfully used for electroanalytical measurements, there are some drawbacks that limit more widespread application. One of these is the high temperature required (600−800 °C) for deposition, which limits the substrates that can be used.

One class of carbons that has been comparatively unstudied in terms of their electrochemical properties and electroanalytical performance is diamond-like carbon.[10−14] These are composite materials consisting of a mixture of sp^2- and sp^3-bonded carbon. Impurities can be incorporated during growth (e.g., N) further adding to their complex structure. Tetrahedral amorphous carbon (ta-C) is one material that has received study over the years.[11] These films typically possess 40−60% sp^3-bonded carbon. It has been widely used as a protective coating because of its hardness, high wear resistance, and low coefficient of friction. The growth temperature for ta-C is usually from 25 to about 100 °C. This means that nontraditional materials, such as plastics, can be used as substrates for deposition. The ta−C films generally need to be grown thin (100s of nanometers) in order to minimize internal stress. Stressed films tend to delaminate from a substrate.

There have been a few reports describing the basic electrochemical properties of ta-C and ta-C:N films as well as their application in electroanalytical measurements.[15−28] The pioneering work was reported by the Miller lab at Case Western Reserve University. They demonstrated that ta-C:N films exhibit a wide working potential window in aqueous media (>3 V), good activity for $Ru(NH_3)_6^{+3/+2}$, and microstructural stability during chlorine electrolysis.[19] In other work, for example, the detection of dopamine and ascorbate with ta-C:N films has been described. The ta-C:N films provide improved sensitivity and linear dynamic range compared to other electrodes.[23] More recently, Tanaka et al. reported that nitrogen-doped hydrogenated amorphous carbon thin films (a-C:N:H) function as an ideally polarizable electrode material with a wide working potential window, low double-layer capacitance, and high stability in strong acid. $Fe(CN)_6^{3-/4-}$ and $Ru(NH_3)_6^{2+/3+}$ electrode kinetics were reported on.[28] Even with these published works, there is still an incomplete understanding of structure−function relationships at these interesting electrode materials. Our work is focused on addressing this knowledge gap.

The overall goal of this work is to determine the microstructure of the ta-C and ta-C:N films, as deposited by pulsed laser-arc deposition, and to correlate the film microstructure with the basic electrochemical properties. We tested

Received: May 9, 2012
Accepted: June 18, 2012
Published: June 18, 2012

the hypothesis that increased nitrogen incorporation would result in a greater fraction of sp^2-bonded carbon in the films and that this would cause the electrochemical properties of the films to transition from ones more resembling diamond (sp^3 carbon) to ones more resembling glassy carbon (sp^2 carbon).[29] The film chemistry was probed by XPS, while the film microstructure was characterized by EELS and Raman spectroscopy. The heterogeneous electron-transfer kinetics for $Ru(NH_3)_6^{+3/+2}$ and $Fe(CN)_6^{-3/-4}$ were studied as was the potential-dependence of the electrode capacitance. The tendency for a redox-active molecule, methylene blue, to adsorb was investigated as a function of the film microstructure.

EXPERIMENTAL SECTION

The experimental details can be found in the Supporting Information.

RESULTS

XPS Analysis. Details of the XPS analysis are included in the Supporting Information (Figure S-1A–C). Evidence was found for the presence of some sp^3 carbon in these films on the basis of the C1s line position.[30] A near-linear relationship was found between the amount of nitrogen incorporated and the N_2 flow rate (Figure S-1C of the Supporting Information). The N/C atomic ratio increased from 0% for a film grown without N_2 to 6% for the film grown with 10 sccm N_2 and finally to 13% for the film deposited with 50 sccm N_2. We presume that these near-surface levels are reflective of the atomic composition throughout the film bulk as all are relatively thin (~200 nm thick). All the films, regardless of the nitrogen content, contain a relatively constant O/C atomic ratio of 13–15% in the near-surface region.

Electron Energy Loss Spectroscopy (EELS). Small-spot EELS measurements were made to assess the local carbon bonding in ta-C films with different levels of incorporated nitrogen. The carbon K-edge spectra for the ta-C and ta-C:N films are presented in Figure 1A. Figure 1B presents characteristic reference spectra for a pure sp^3 carbon material, diamond, and a pure sp^2 material, multiwall carbon nanotubes (MWCNTs). Unlike the reference spectrum for diamond that consists of a well-defined σ^* absorption edge at 289.5 eV and a second bandgap feature at about 302.0 eV, the spectra for the ta-C and ta-C:N films all consist of a π^* peak at 285.4 eV that arises from the sp^2-bonded carbon domains, as well as a broad and more intense sp^3 carbon σ^* absorption edge. The spectrum for each of the films is characteristic of a mixed-microstructure l (sp^2/sp^3) material.

The curve area between 280 and 285.4 eV is reflective of the amount of sp^2-bonded carbon (π) in the probed region, while the curve area from 285.4 to 292.4 eV is indicative of the sp^3-bonded carbon (σ) content.[31,32] Therefore, the σ/π area ratio provides an estimate of the sp^3 relative to the sp^2-bonded carbon content in the films. Spectra were obtained from 10 random spots on each film, and the area ratios were averaged together to produce the data displayed in Table 1. As shown, the fraction of sp^2-bonded carbon increases with increasing nitrogen incorporation. These ta-C and ta-C:N films have an sp^3/sp^3+sp^2 carbon content that ranges from 60 to 40%, decreasing with increasing nitrogen incorporation. The nominal σ/π area ratio is 1.3 for the 0 and 10 sccm N_2 films and decreases to 0.97 and 0.72, respectively, for the 30 and 50 sccm N_2 films. This is consistent with the published reports for ta-C:N films.

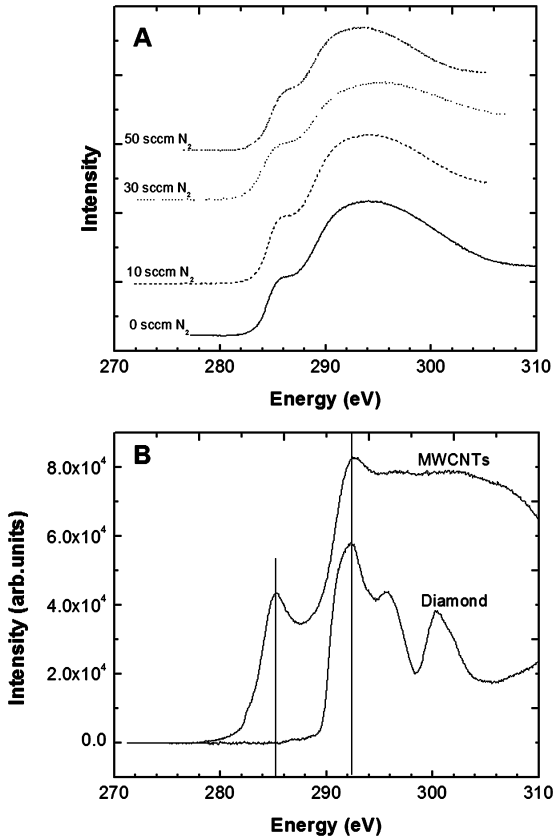

Figure 1. (A) Electron energy loss spectra (EELS) at the C K edge for ta-C films deposited with 0, 10, 30, and 50 sccm N_2. (B) Reference spectra for single-crystal diamond (pure sp^3) and multiwall carbon nanotubes (pure sp^2).

Table 1. Summary of EELS Data for the ta-C Films Deposited with 0, 10, 30, and 50 sccm N_2[a]

% carbon bonding	0 sccm N_2	10 sccm N_2	30 sccm N_2	50 sccm N_2
sp^2	44 ± 3	44 ± 9	51 ± 8	58 ± 9
sp^3	56 ± 3	56 ± 9	49 ± 8	42 ± 9

[a]Data generated from 10 measurements made randomly on each film.

Atomic Force Microscopy. Figure S-2 of the Supporting Information presents height-mode AFM images (3 μm × 3 μm) for the ta-C and ta-C:N films. On the basis of the image features, all the films are characterized by a nodular morphology. The nodular features increase in size with increasing nitrogen content. This contributes to an increasing film roughness. Five measurements (3 μm × 3 μm) were made at different locations on each film to determine the roughness. The nominal roughness of each film type was 9 ± 4 (0 sccm N_2), 15 ± 7 (10 sccm N_2), 14 ± 3 (30 sccm N_2), and 23 ± 9 nm (50 sccm N_2). Clustering of the nitrogen in the films and the surrounding carbon growth may contribute to the nodule formation.

Visible Raman Spectroscopy. Raman spectroscopy was used to assess the film microstructure over a larger dimension (μm) than the EELS measurements. The data are presented in Figure S-3 of the Supporting Information. The spectra are characterized by a broad, asymmetric scattering profile between 1000 and 1700 cm^{-1}, with a single peak maximum at about

1510 cm^{-1}. Such spectra are typical for ta-C films.[33] The peak becomes more asymmetric with increasing nitrogen incorporation as the scattering intensity near 1350 cm^{-1} increases. This trend is indicative of an increasing fraction of sp^2-bonded carbon. The Raman spectrum for amorphous carbons, like ta-C, is dominated by modes of the graphitic lattice; the so-called D and G modes.[34] This domination is because of the sizably larger (230X) scattering cross-section coefficient for the sp^2-bonded carbon.[35,36] The G mode for amorphous carbons arises from the bond stretching vibrations of pairs of sp^2 sites, and the D mode is due to the breathing mode of six-fold sp^2 rings.[37]

To estimate the sp^2/sp^3 carbon ratio in the films, the spectra were fit with two Gaussian−Lorentzian peaks: the D-mode centered at 1358 cm^{-1} and the G-mode at 1580 cm^{-1}.[33] An example of the peak fitting is presented in Figure S-3 of the Supporting Information for the 50 sccm ta-C:N film. Table 2 presents a summary of the I_D/I_G peak intensity ratio, the G-band position, and the peak widths for the different ta-C films. These parameters were determined from the spectral fitting. Robertson et al.[38] reported that the I_D/I_G intensity ratio and the line width of G peak are good indicators of the Ta:C film microstructure. It can be seen that the I_D/I_G ratio increases with increasing N content. The G-mode width also decreases and the band position shifts to lower wave numbers with increasing N content. Both are the expected trends for increasing sp^2 carbon content and/or domain size. The Raman data, along with the EELS results, confirm that the ta-C films with increasing nitrogen levels have increased levels of sp^2-bonded carbon.

Table 2. Raman Spectral Paramenters for ta-C and ta-C:N Films Obtained from Fitting the Spectra with Two Peaks Using Gaussian-Lorentizian Functions: D-band at 1358 cm^{-1} and G-band at 1580 cm^{-1}[a]

sample	I_D/I_G	G-band position (cm^{-1})	fwhm, W_G (cm^{-1})
ta-C	0.64 ± 0.02	1556.6 ± 1.2	172.4 ± 1.6
10 sccm N_2 ta-C:N	0.84 ± 0.02	1552.6 ± 0.7	164.4 ± 3.2
30 sccm N_2 ta-C:N	0.99 ± 0.09	1548.2 ± 0.9	163.4 ± 2.2
50 sccm N_2 ta-C:N	1.12 ± 0.05	1547.0 ± 1.9	158.0 ± 0.6

[a]The ta-C:N films were deposited with 10, 30, and 50 sccm N_2; (n = 4).

Electrochemical Performance. Figure 2 shows background cyclic voltammetric *i-E* curves for the ta-C and ta-C:N films in 1 M KCl. Curves for glassy carbon and boron-doped diamond are also presented for comparison. The geometric area of all the electrodes was 0.2 cm^2. The curves for all the films are featureless with current magnitudes slightly higher than the current for the boron-doped diamond film but lower than the current for glassy carbon. For example, at 0.2 V, the anodic current for diamond is 4.5 $\mu A/cm^2$. In contrast, the current for glassy carbon is 5 times larger at 23.1 $\mu A/cm^2$. For all the ta-C and ta-C:N films, the background current at this potential is approximately 12 $\mu A/cm^2$. The lower background current for the ta-C and ta-C:N films is an attractive feature for electroanalytical measurements in terms of enhanced S/B ratios.

Figure 3 shows capacitance−potential (C_{dl}-E) profiles for each of the ta-C and ta-C:N films recorded in 1 M KCl.

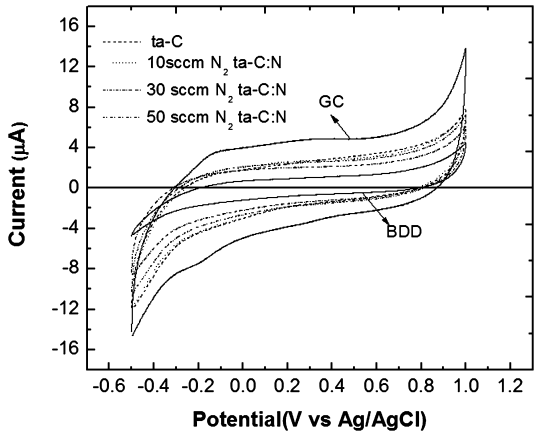

Figure 2. Cyclic voltammetric *i-E* curves for ta-C, ta-C:N films grown with 10, 30, and 50 sccm N_2, glassy carbon, and a boron-doped diamond (BDD) thin film, all in 1 M KCl. Scan rate = 0.1 V/s. Geometric area = 0.2 cm^2.

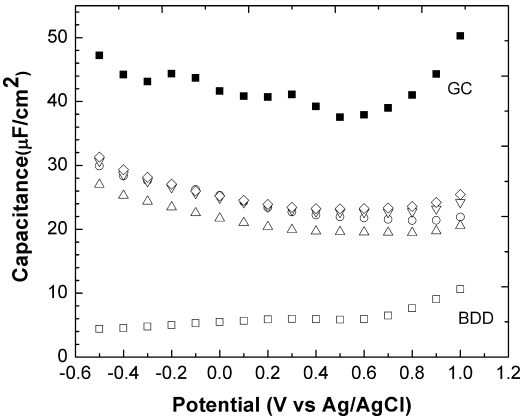

Figure 3. Capacitance−potential profiles for ta-C (○), 10 sccm N_2 ta-C:N (△), 30 sccm N_2 ta-C:N (▽), and 50 sccm N_2 ta-C:N (◇) films in 0.1 M $HClO_4$. Comparison data for glassy carbon and boron-doped diamond are presented. Capacitance values were determined using a 10 mV rms sine wave at 40 Hz. $Z_{im} = 1/(2\pi f C_{dl})$. Data are normalized to the geometric area, 0.2 cm^2.

Comparison data are presented for glassy carbon and boron-doped diamond. The capacitance for glassy carbon ranges from 35 to 50 $\mu F/cm^2$ over the potential range probed is higher than previously reported data by our group for polished glassy carbon.[39] We attribute this to increased surface roughness. In contrast, the capacitance for boron-doped diamond ranges from 5 to 11 $\mu F/cm^2$, consistent with our previously reported results.[39] The capacitance of the ta-C films falls in between with values of 20−30 $\mu F/cm^2$. This suggests that the electronic properties of these electrodes lie intermediate between those of a semimetal, like diamond, and a conductor, like glassy carbon.

Figure 4A shows cyclic voltammetric *i-E* curves for a ta-C film in 0.5 M H_2SO_4 before (solid line) and after the film was anodically polarized (dotted line). The purpose for this measurement was to determine the stability of the ta-C microstructure during a typical anodic polarization pretreatment that might be used to activate glassy carbon. One of the characteristics of diamond is its superb microstrucutural stability during exposure to aggressive electrochemical conditions.[40] The polarization was carried out potentiostatically at 2 V vs Ag/AgCl for 15 min in 0.5 M H_2SO_4 (25 °C).

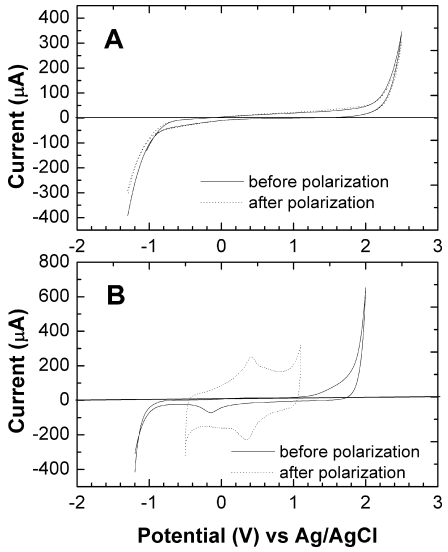

Figure 4. Cyclic voltammetric *i-E* curves for (A) ta-C film and (B) glassy carbon in 0.5 M H_2SO_4 before polarization and after polarization. Scan rate = 50 mV/s. Geometric area = 0.2 cm^2.

Comparison curves for freshly glassy carbon, before and after an identical polarization, are presented in Figure 4B. The curve for the ta-C film prior to polarization is featureless within the working potential window (~3 V). The background current is low and relatively constant with potential. Similar curve shapes were observed for the other ta-C:N films prior to anodic polarization (data not shown). The working potential window (defined as ±300 μA) for the ta-C film is 3.1 V, which is lower than the value for boron-doped diamond in this same electrolyte solution (~3.5 V) but larger than the value for glassy carbon (~2.7). The nominal potential windows for the ta-C and ta-C:N films (10, 30, and 50 sccm N_2) were 3.13 ± 0.09, 3.07 ± 0.05, 2.89 ± 0.05, and 2.78 ± 0.08, respectively. Clearly, the potential window decreases with increasing nitrogen content, and this correlates with increasing sp^2 carbon content in the films. The comparison voltammetric behavior of glassy carbon is distinct. The background current (same geometric area) within the working potential window is 3−6 times greater than the ta-C films.

The anodic polarization changes the voltammetric behavior of glassy carbon considerably while imparting virtually no change to the response of the ta-C and ta-C:N films. For the ta-C and ta-C:N films, the working potential window and the background current within the window were unaffected by the anodic polarization. In contrast, a significant increase in the background current and a reduction in the working potential window were observed for glassy carbon. These trends are caused by the microstructural damage (exposure of clean edge plane sites) and surface oxidation caused by the polarization. Well-defined redox peaks develop at 0.2 V for glassy carbon. These peaks are associated with electroactive surface-carbon oxygen functionalities (i.e., quinone−hydroquinone surface couple), and these groups represent some fraction of the total oxides produced by the polarization.[1] For glassy carbon, the total anodic charge passed was largest at 2.1 ± 0.4 C/cm^2. In comparison, the charge passed for the ta-C and ta-C:N film deposited with 10 sccm N_2 was identical: 0.13 ± 0.1 C/cm^2.

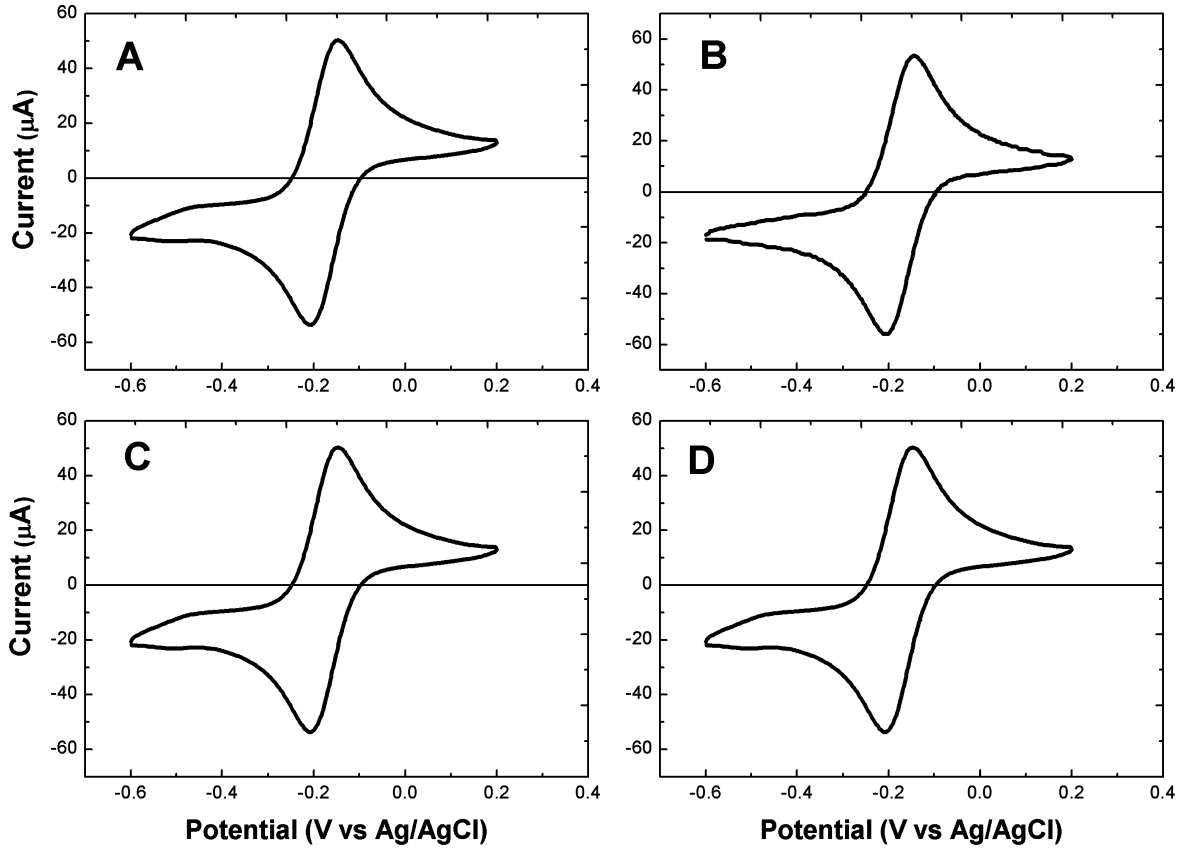

Figure 5. Cyclic voltammetric *i-E* curves for (A) ta-C, (B) 10 sccm N_2, (C) 30 sccm N_2, and (D) 50 sccm N_2 ta-C:N films in 1 mM $Ru(NH_3)_6^{2+/3+}$ + 1 M KCl. Scan rate = 0.1 V/s. Geometric area = 0.2 cm^2.

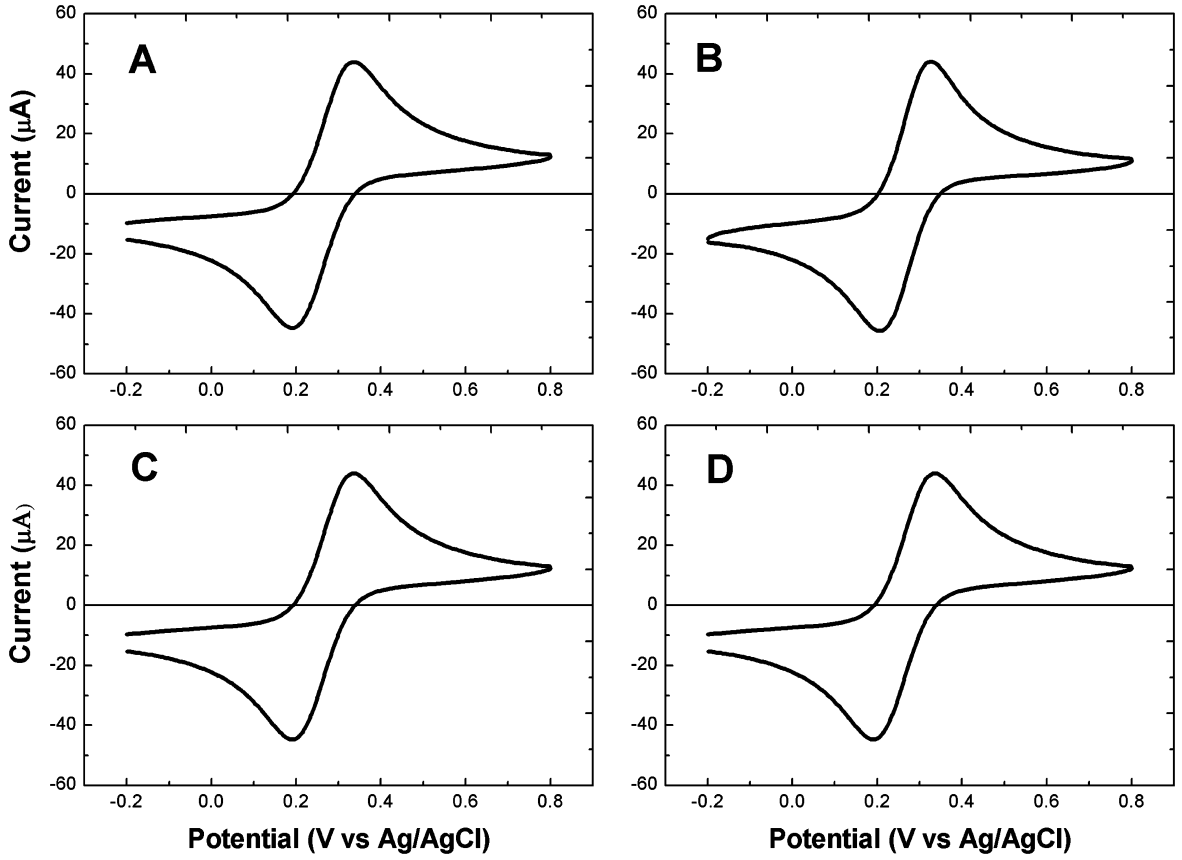

Figure 6. Cyclic voltammetric *i-E* curves for (A) ta-C, (B) 10 sccm N_2, (C) 30 sccm N_2, and (D) 50 sccm N_2 ta-C:N films in 1 mM $Fe(CN)_6^{3-/4-}$ in 1 M KCl. Scan rate = 0.1 V/s. Geometric area = 0.2 cm^2.

Table 3. Summary of Cyclic Voltammetric Data for $Ru(NH_3)_6^{+3/+2}$ and $Fe(CN)_6^{-3/-4}$ at ta-C and ta-C:N Thin Films Deposited with 10, 30, and 50 sccm N_2[a]

	ta:C N−ta:C	10 sccm N_2 N−ta:C	30 sccm N_2 N−ta:C	50 sccm N_2
$Ru(NH_3)_6^{2+/3+}$				
ΔE_p (mV)	58 ± 1	59 ± 3	61 ± 3	59 ± 5
i_p^{red} (μA)	55 ± 2	60 ± 3	58 ± 1	58 ± 1
$Fe(CN)_6^{3-/4-}$				
ΔE_p (mV)	119 ± 18	109 ± 17	97 ± 6	84 ± 15
i_p^{ox} (μA)	49 ± 4	52 ± 4	54 ± 2	53 ± 7
k^o(cm/s)	0.005 ± 0.001	0.006 ± 0.002	0.008 ± 0.001	0.015 ± 0.009
α	0.5	0.5	0.5	0.5

[a]Scan rate = 0.1 V/s. Geometric area = 0.2 cm^2; (n = 5).

The 10 times lower charge, compared to glassy carbon, results because of the resistance of ta-C films to microstructural damage and surface oxidation as well as the wider potential window such that there is less contributed charge from water electrolysis. Interestingly though, the charge passed for the ta-C:N film deposited with 30 sccm N_2 was 0.43 ± 0.08 C/cm^2, about 3−4 times greater than the ta-C film, while the charge passed during polarization of the ta-C:N film deposited with 50 sccm N_2 was even greater at 2.0 ± 0.01 C/cm^2, nearly identical to that passed for glassy carbon. Even though the total charge passed for this film was close to that for glass carbon, the working potential window and the background current for the 50 sccm ta-C:N film were still largely unaltered.

Figures 5 and 6 show cyclic voltammetric *i-E* curves for the ta-C and ta-C:N films in the presence of 1 mM $Ru(NH_3)_6^{2+/3+}$ and 1 mM $Fe(CN)_6^{3-/4-}$, respectively, both in 1 M KCl. Table 3 provides a statistical summary of the cyclic voltammetric data for all four electrodes and presents apparent heterogeneous electron-transfer rate constants, k^o_{app}. $Ru(NH_3)_6^{2+/3+}$ is classified as an outer-sphere redox couple and generally involves simple electron transfer at carbon electrodes. k^o for this redox couple is relatively insensitive to the surface microstructure, surface oxides, and the adsorbed monolayers on sp^2 carbon electrodes.[3,41,42] The heterogeneous electron-transfer rate constant is mainly controlled by the electronic properties of the electrode (i.e., carrier mobility and carrier concentration). Well-defined peak-shaped curves are seen for all the films. Essentially reversible (Nernstian) behavior is seen as the peak separation potential, ΔE_p, and is 59 mV for all four films. Plots of i_p^{red} vs $\nu^{1/2}$ were linear for all four films between

0.1 and 0.7 V/s (R^2 > 0.99), which indicates the current is controlled by semi-infinite linear diffusion of the analyte to the electrode surface. The i_p^{ox}/i_p^{red} ratios were near unity for all four electrodes confirming the chemical reversibility of the redox reaction. Near Nernstian behavior was observed for this redox system at all the ta-C films at the scan rates employed. Therefore, we were unable to extract k^o_{app} values from the data as the system was behaving reversibly.

$Fe(CN)_6^{3-/4-}$, on the other hand, is an inner-sphere redox couple with a k^o value that is strongly influenced by several variables: (1) the electronic properties of the electrode (density of electronic states near E^0), (2) surface cleanliness, and (3) surface chemistry (e.g., carbon−oxygen functional groups).[3,41,42] As shown in Table 3, the ΔE_p values decrease with increasing N content. Well-defined peak-shaped curves are seen for all four films. The i_p^{ox} vs $\nu^{1/2}$ plots were linear for all four films between 0.1 and 0.7 V/s (R^2 > 0.99). The i_p^{ox}/i_p^{red} ratios were unity. The k^o_{app} value increases with nitrogen content ranging from 0.005 ± 0.001 cm/s for the ta-C film to 0.015 ± 0.009 cm/s for the 50 sccm ta-C:N film.

Microstructural Stability: Effect of Chemical Oxidation. The microstructure of the different ta-C and ta-C:N films was unaffected by the anodic polarization (Figure 4). The stability and performance of the films were also evaluated during strong chemical oxidation. This oxidation treatment is often used to clean diamond surfaces without causing any microstructural alteration. The chemical oxidation involved two steps: (i) 20 min in 3:1 (v/v) HNO_3:HCl at ∼55 °C and (ii) 20 min in a 30% H_2O_2 solution at ∼55 °C. In the case of the ta-C or the ta-C:N films grown with 10 and 30 sccm of N_2, the oxidation did not alter the microstructure or affect the basic electrochemical properties. However, the 50 sccm N_2 ta-C:N film was completely destroyed by the oxidation as the film cracked and delaminated from the Si substrate.

For the intact films, the voltammetric background current in 1 M KCl increased only by a factor of 1.0−1.5 times after the chemical oxidation. The background anodic current at 0.2 V for all the films increased linearly with the scan rate from 0.1 to 0.5 V/s (R^2 > 0.99), as expected for capacitive current. From the slope of the i_{bk} vs υ plots, the capacitance, C_{dl}, was determined to be 58, 42, and 56 μF/cm^2, respectively, for the ta-C, and the 10 and 30 sccm N_2 ta-C:N films. The apparent capacitance increase after oxidation is likely due to surface oxidation that increases the surface wettability and causes roughening. We did not interrogate these films by AFM or SEM to verify the surface roughening. In summary, with the exception of the 50 sccm N_2 film (i.e., the greatest sp^2 carbon content), the morphology and microstructure of the ta-C and ta-C:N films are stable, like boron-doped diamond, during exposure to this aggressive chemical oxidation.

With the exception of the 50 sccm N_2 ta-C:N film, the electrochemical response of the films toward $Ru(NH_3)_6^{+3/+2}$ was largely unchanged after the chemical oxidation. After oxidation, ΔE_p for $Ru(NH_3)_6^{+3/+2}$ increased only from 59 to 65 mV (near Nernstian) up to 0.5 V/s. The i_p^{red} vs $\nu^{1/2}$ plots remained linear. The effect of oxidation on the $Fe(CN)_6^{-3/-4}$ response was distinctly different. ΔE_p values increased for all three films after oxidation compared to those values presented in Table 3, which are consistent with more sluggish electron-transfer kinetics. For the ta-C film, ΔE_p increased from 167 to 314 mV between 0.1 to 0.5 V/s, from 91 to 145 mV for the 10 sccm ta-C:N film, and from 91 to 120 mV for the 30 sccm ta-C:N film. For all three, i_p^{ox} vs $\nu^{1/2}$ plots remained linear.

Voltammetric Behavior of Methylene Blue. Methylene blue is an electroactive molecule that strongly adsorbs on glassy carbon electrode surfaces.[3,42] The theoretical monolayer surface coverage of methylene blue is 190 pmol/cm^2. We therefore selected this molecule as a probe for molecular adsorption on the ta-C films. The cyclic voltmmetric *i-E* curves in 10 μM methylene blue are shown in Figure 7 for glassy carbon and a 30 sccm N_2 ta-C:N film. The solid line represents the background current in 0.1 M H_2SO_4. The "in solution" cyclic voltmmetric *i-E* curves were obtained in the presence of 10 μM methylene blue. The "after soaking" curves were obtained after cycling the electrode in the presence of methylene blue for multiple minutes, removing the solution and rinsing the electrode, and replacing the solution with 0.1 M H_2SO_4.

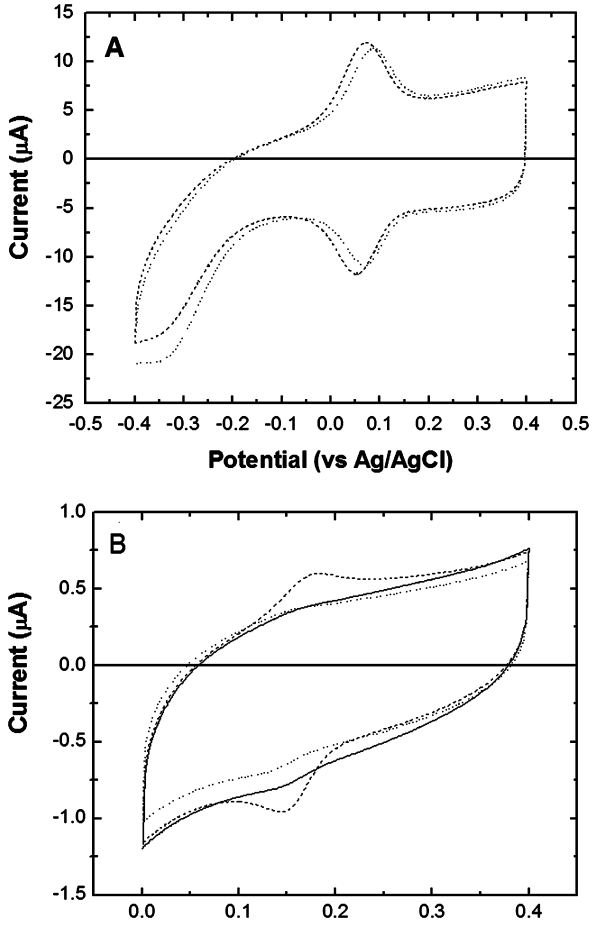

Figure 7. Cyclic voltammetric *i-E* curves for (A) glassy carbon and (B) a 30 sccm N_2 ta-C:N film in 0.1 M H_2SO_4 (—), in 10 μM methylene blue solution (---), and after soaking and rinsing (···). Scan rate = 0.025 V/s. Geometric area = 0.2 cm^2. Note the difference in potential range on the *x*-axes.

The cyclic voltammogram for glassy carbon showed characteristic features of methylene blue adsorption.[3] A pair of narrow symmetric peaks is shown with a ΔE_p of 16 mV. This is close to the theoretical value of ΔE_p = 0 expected for an admolecule undergoing rapid electron-transfer kinetics. The theoretical diffusion-limited peak current was calculated to be 0.15 μA for this solution concentration (n = 2, A = 0.2 cm^2, ν = 0.025 V/s, and D = 3 × 10^{-6} cm^2/s). The oxidation peak current, i_p^{ox} (Figure 7A) is 7.1 μA or ∼47 times larger than the theoretical value. This is consistent with adsorbed methylene

dx.doi.org/10.1021/ac301124r | Anal. Chem. 2012, 84, 6240−6248

blue. Additionally, the peak currents increased proportionally with the scan rate (0.025−0.1 V/s, $R^2 > 0.98$), consistent with adsorbed redox molecule. The surface coverage calculated from the anodic peak charge was 335 pmol/cm^2. Solution immersion testing was also performed. After immersing the glassy carbon surface in the 10 μM methylene blue solution, rinsing the surface, and replacing the solution with fresh 0.1 M H_2SO_4, a cyclic voltammetric curve nearly identical to that in Figure 7A was obtained. Integration of the anodic peak charge lead to a calculated coverage of 399 pmol/cm^2.

In contrast, for the 30 sccm ta-C:N film, there was no evidence for molecular adsorption. Immersion tests revealed the absence of adsorption as the cyclic voltammetric *i-E* curves in 0.1 M H_2SO_4 after methylene blue exposure were devoid of any redox peaks. The oxidation peak current, i_p^{ox}, in Figure 7B is 0.14 μA, which is very close to the theoretical value of 0.15 μA for a diffusion controlled process. The i_p^{ox} values increased linearly with $\nu^{1/2}$ ($R^2 > 0.99$) consistent with a diffusion controlled redox reaction. Three different 30 sccm ta-C:N films were tested with identical results for all.

DISCUSSION

Structurally, it was found that the ta-C and ta-C:N films possess a mixed sp^3- and sp^2-bonded carbon microstructure. The sp^3/sp^3+sp^2 content varied between 40 and 60%, decreasing with increasing incorporated nitrogen. It is unclear if the sp^2-bonded carbon exists as 6-membered rings, linear or branched chains of unsaturated hydrocarbons, or some combination of the two. Both the EELS and Raman spectroscopic data confirmed the existence of sp^2 carbon domains. The near-surface N/C atomic ratio, as determined by XPS, increased linearly with the process gas N_2 flow from 0 (undetectable nitrogen) for the ta-C film to 14% for the 50 sccm N_2 ta-C:N film. Oxygen was present on all film surfaces at a constant level of about 14% (O/C). Given the film thickness, ∼200 nm, we suppose that the near-surface elemental composition is reflective of the bulk composition. With increasing nitrogen content, the fraction of sp^2 carbon in the film increased. The incorporated nitrogen likely forms sp^2 hybridized bonds with carbon (C═N) and this leads to an overall increase in the sp^2 carbon content. The film roughness also increased with the nitrogen content. We do not know from our data exactly how the nitrogen is bonded within the films. Future FTIR studies will hopefully provide greater insight as to the C−N bonding in the films.

The electrochemical data indicated the ta-C and low nitrogen ta-C:N thin-film electrodes have properties more similar to those of boron-doped diamond than to those of glassy carbon. Background cyclic voltammetric currents were lower than those for glassy carbon by a factor of 2−5 times but slightly higher than those for diamond. The background currents increased slightly with increasing nitrogen content, consistent with increasing sp^2 carbon content. The capacitance values for the ta-C and ta-C:N films were intermediate between those of diamond and glassy carbon. Capacitance values for all the ta-C films ranged from 20 to 30 μF/cm^2 in 0.1 M $HClO_4$ between −0.5 and 1.0 V vs Ag/AgCl. There was not a major difference in the values for the different films, regardless of the nitrogen (i.e., sp^2 carbon) content. This suggests that the electronic properties are not significantly altered by the change in sp^2 bonding within the films. The lower capacitance and background voltammetric current of the ta-C films make this electrode material attractive for electroanalytical measurements in terms of increased signal-to-background ratios. We are presently investigating the use of these materials in flow injection analysis coupled with electrochemical detection in order to determine what analytical detection figures of merit are possible.

The working potential window for the ta-C films in 0.5 M H_2SO_4 ranged from 3.1 V for the film deposited with no added N_2 to 2.8 V for the ta-C:N film deposited with 50 sccm N_2. By way of comparison, the potential window for glassy carbon in the same medium is 2.7 V. As is the case for microcrystalline and ultrananocrystalline diamond, the background current increases and the working potential window decreases with increasing sp^2 carbon content.[43,44] The 2.8 V limit for the 50 sccm ta-C:N film is similar to the 2.7 V limit for glassy carbon. The sp^2-bonded graphitic carbons, with a high fraction of exposed edge plane, are more kinetically active for solvent breakdown (oxygen evolution and hydrogen evolution from water) than is diamond. Therefore, increasing the sp^2 carbon content in these a ta-C films causes a proportional decrease in the working potential window and an increase in the voltammetric background current.

With the exception of the glassy carbon-like 50 sccm ta-C:N film, the other ta-C and ta-C:N films exhibited excellent microstructural stability during anodic polarization and harsh chemical oxidation, much like boron-doped diamond. These are trademark characteristics of diamond that are mimicked for the most part by these ta-C films. The surface also does not undergo extensive surface oxide formation, at least ionizable and or electrochemically active oxides, during either of these two treatments as evidenced by the fact that the background voltammetric current and working potential window are both relatively unchanged after treatment. The ta-C:N film deposited with 50 sccm N_2 behaved more like a graphitic carbon being completely destroyed during exposure to two-step oxidation treatment. The greater sp^2 carbon content of this film rendered it more susceptible to microstructural degradation, likely due to the corrosion (gasification) of this carbon preferentially over the sp^3 carbon.

The ta-C and ta-C:N films support relatively rapid electron-transfer rates for $Ru(NH_3)_6^{+3/+2}$ and $Fe(CN)_6^{-3/-4}$. The reproducibility of the voltammetric responses from film to film was also very good. The cyclic voltammetric response for $Ru(NH_3)_6^{+3/+2}$ was Nernstian for all the films with ΔE_p values of about 59 mV at scan rates from 0.1 to 0.5 V/s. There was no increase in ΔE_p with increasing analyte concentration in solution (same scan rate, indicating that ohmic resistance within the films was not influencing the *i-E* curve shapes. The apparent heterogeneous electron-transfer rate constant for this redox system at all the films was greater than 0.1 cm/s, which is comparable to what has been reported for boron-doped microcrystalline and ultrananocrystalline diamond thin films.[44,45] In other words, the activity of the ta-C and ta-C:N films for this redox system is independent of the sp^2 carbon content, similar to what has been observed for boron-doped diamond.[43]

In contrast, quasireversible electron-transfer kinetics were seen for $Fe(CN)_6^{-3/-4}$ at all the films. ΔE_p values decreased with increasing nitrogen content (i.e., increasing sp^2 carbon content), ranging from a nominal value of 119 mV for the ta-C film to 84 mV for the 50 sccm N_2 ta-C:N film. Clearly, the sp^2-bonded carbon introduces more active sites for this redox system, and the trend is not a reduction in the ohmic resistance of the film on the basis of the $Ru(NH_3)_6^{+3/+2}$ data. The resistivity of the ta-C:N films were similar for the 10, 30, and 50

sccm N_2 levels: 6.62 ± 0.98, 1.49 ± 0.07, and 1.10 ± 0.07 Ω-cm, respectively. The data were obtained using thin films grown on quartz. The trend seen for the ta-C films is similar to that seen for boron-doped diamond electrodes with increasing levels of sp^2 carbon impurity. These two distinct redox analyte behaviors are why the electrochemical activity of these new carbon electrodes must be evaluated using a variety of redox systems. The reason for the $Fe(CN)_6^{-3/-4}$ activity increase with increasing sp^2 carbon content is unclear at this time but may be related to (i) increases in active site density[46,47] and or (ii) differences in the double layer structure (potential at the plane of closest approach) at the sp^3 versus the sp^2 carbon sites, which have a greater impact on the inner-sphere $Fe(CN)_6^{-3/-4}$ redox couple.[48] The apparent heterogeneous electron-transfer rate constants ranged from 0.005 to 0.015 cm/s, which are comparable to those found for diamond.[45]

The undetectable methylene blue adsorption on the ta-C and ta-C:N films is certainly a distinguishing feature and very much resembles the characteristics of boron-doped diamond. The strong molecular adsorption on glassy carbon is likely driven by a combination of H-bonding, dipole−dipole, and $\pi-\pi$ interactions at the electrode surface. While the 30 sccm ta-C:N film has surface carbon−oxygen functional groups, the types of functional groups and the functional group density are likely different from glassy carbon. For example, there is no evidence for any redox-active quinone functional groups on the ta-C films like there are on oxidized glassy carbon (see peaks in Figure 4B). Also, the ta-C:N films possess no extended π-electron system. Taken together, these differences are likely the reason for the weak molecular adsorption of methylene blue on the ta-C electrodes.

As a final point, it is worth noting the ta-C and ta-C:N films exhibit some similarities with the nanocarbon films from Niwa's group, which have sp^3/sp^2+sp^3 about 0.70.[49−52] Their electron cyclotron resonance (ECR)-sputtered carbon films exhibit a wide working potential window (3.7 V in 0.05 M H_2SO_4) and rapid electron-transfer for $Ru(NH_3)_6^{+3/+2}$ and $Fe(CN)_6^{-3/-4}$.

CONCLUSIONS

The ta-C and ta-C:N films were synthesized by pulsed laser-arc deposition with 40−60% sp^3 carbon. The fraction of sp^2 carbon in the films increased with the level of nitrogen incorporated. In many respects, the ta-C and ta-C:N films (10 and 30 sccm N_2) exhibit electrochemical properties more resembling those of boron-doped diamond than those of glassy carbon. These films exhibit a comparatively low voltammetric background current, a wide working potential window, stability to microstructural damage during exposure to strong oxidants and aggressive electrochemical conditions, relatively rapid electron-transfer kinetics for $Ru(NH_3)_6^{+3/+2}$ and $Fe(CN)_6^{-3/-4}$, and weak adsorption of methylene blue. As the nitrogen content in the films increased (i.e., increased sp^2 carbon content), the background current increased, the working potential window decreased, and the electron-transfer kinetics for $Fe(CN)_6^{-3/-4}$ increased. Overall, the properties of the ta-C and ta-C:N electrodes are such that they could be excellent new choices for electroanalytical measurements.

ASSOCIATED CONTENT

Supporting Information

Additional information as noted in text. This material is available free of charge via the Internet at http://pubs.acs.org.

AUTHOR INFORMATION

Corresponding Author

*E-mail: swain@chemistry.msu.edu

Notes

The authors declare no competing financial interest.

ACKNOWLEDGMENTS

This work was supported by a grant from the National Science Foundation (CHE-0911383). Any opinions, findings, and conclusions or recommendations expressed in this paper are those of the author(s) and do not necessarily reflect the views of the National Science Foundation. The authors also thank Dr. Per. Ashland for his assistance with the XPS measurements, Catherine Munson for her help with the methylene blue measurements. and Dr. Akio Ueda (AIST) for his fine contributions during the early stages of this work.

REFERENCES

(1) McCreery, R. L. *Chem. Rev.* **2008**, *108*, 2646.
(2) Rice, R. J.; Pontikos, N. M.; McCreery, R. L. *J. Am. Chem. Soc.* **1990**, *112*, 4617−22.
(3) Chen, P.; Fryling, M. A.; McCreery, R. L. *Anal. Chem.* **1995**, *67*, 3115−22.
(4) Pleskov, Y. V.; Sakharova, A. Y.; Krotova, M. D.; Builov, L. L.; Spitsyn, B. V. *J. Electroanal. Chem. Interfacial Electrochem.* **1987**, *228*, 19−27.
(5) Janssen, G.; Van, E. W. J. P.; Vollenberg, W.; Giling, L. J. *Diamond Relat. Mater.* **1992**, *1*, 789−800.
(6) Swain, G. M.; Ramesham, R. *Anal. Chem.* **1993**, *65*, 345−51.
(7) Alehashem, S.; Chambers, F.; Strojek, J. W.; Swain, G. M.; Ramesham, R. *Anal. Chem.* **1995**, *67*, 2812−2821.
(8) Angus, J. C.; Martin, H. B.; Landau, U.; Evstefeeva, Y. E.; Miller, B.; Vinokur, N. *New Diamond Front. Carbon Technol.* **1999**, *9*, 175−187.
(9) Rao, T. N.; Ivandini, T. A.; Terashima, C.; Sarada, B. V.; Fujishima, A. *New Diamond Front. Carbon Technol.* **2003**, *13*, 79−88.
(10) Grill, A. *Diamond Relat. Mater.* **1999**, *8*, 428−434.
(11) Robertson, J. *Mater. Sci. Eng., R* **2002**, *37*, 129−281.
(12) Robertson, J. *Diamond Relat. Mater.* **2003**, *12*, 79−84.
(13) Robertson, J. *Semicond. Sci. Technol.* **2003**, *18*, S12−S19.
(14) Robertson, J. *Diamond Relat. Mater.* **2005**, *14*, 942−948.
(15) Evstefeeva, Y. E.; Pleskov, Y. V.; Kutsay, A. M.; Bello, I. *Russ. J. Electrochem.* **2005**, *41*, 772−777.
(16) Khun, N. W.; Liu, E.; Guo, H. W. *Electroanalysis* **2008**, *20*, 1851−1856.
(17) Liu, S.; Wang, G.; Wang, Z. *J. Non-Cryst. Solids* **2007**, *353*, 2796−2798.
(18) Yee, N. C.; Shi, Q. F.; Cai, W. B.; Scherson, D. A.; Miller, B. *Electrochem. Solid-State Lett.* **2001**, *4*, E42−E44.
(19) Yoo, K.; Miller, B.; Kalish, R.; Shi, X. *Electrochem. Solid-State Lett.* **1999**, *2*, 233−235.
(20) Yoo, K.; Miller, B.; Kalish, R.; Shi, X. *Proc. - Electrochem. Soc.* **2000**, *99−32*, 440−447.
(21) Yoo, K.; Miller, B.; Shi, X.; Kalish, R. *J. Electrochem. Soc.* **2001**, *148*, C95−C101.
(22) Zeng, A.; Bilek, M. M. M.; McKenzie, D. R.; Lay, P. A. *Diamond Relat. Mater.* **2009**, *18*, 1211−1217.
(23) Sopchak, D.; Miller, B.; Kalish, R.; Avyigal, Y.; Shi, X. *Electroanalysis* **2002**, *14*, 473−478.
(24) Zeng, A.; Liu, E.; Tan, S. N.; Zhang, S.; Gao, J. *Electroanalysis* **2002**, *14*, 1294−1298.
(25) Zeng, A.; Bilek, M. M. M.; McKenzie, D. R.; Lay, P. A. *Diamond Relat. Mater.* **2009**, *18*, 1102−1108.
(26) Zeng, A.; Liu, E.; Tan, S. N.; Zhang, S.; Gao, J. *Electroanalysis* **2002**, *14*, 1110−1115.

(27) Zhang, W.; Xia, Y.; Ju, J.; Wang, L.; Fang, Z.; Zhang, M. *Solid State Commun.* **2003**, *126*, 163−166.
(28) Tanaka, Y.; Furuta, M.; Kuriyama, K.; Kuwabara, R.; Katsuki, Y.; Kondo, T.; Fujishima, A.; Honda, K. *Electrochim. Acta* **2010**, *56*, 1172−1181.
(29) Show, Y.; Swope, V. M.; Swain, G. M. *Diamond Relat. Mater.* **2009**, *18*, 1426−1434.
(30) Lascovich, J. C.; Giorgi, R.; Scaglione, S. *Appl. Surf. Sci.* **1991**, *47*, 17−21.
(31) Waidmann, S.; Knupfer, M.; Fink, J.; Kleinsorge, B.; Robertson, J. *Diamond Relat. Mater.* **2000**, *9*, 722−727.
(32) Waidmann, S.; Knupfer, M.; Fink, J.; Kleinsorge, B.; Robertson, J. *J. Appl. Phys.* **2001**, *89*, 3783−3792.
(33) Ferrari, A. C.; Rodil, S. E.; Robertson, J. *Phys. Rev. B* **2003**, *67*, 155306.
(34) Ferrari, A. C.; Robertson, J. *Phys. Rev. B* **2001**, *64*, 075414.
(35) Sails, S. R.; Gardiner, D. J.; Bowden, M.; Savage, J.; Rodway, D. *Diamond Relat. Mater.* **1996**, *5*, 589−591.
(36) Wada, N.; Gaczi, P. J.; Solin, S. A. *J. Non-Cryst. Solids* **1980**, *35*−*36*, 543−8.
(37) Ferrari, A. C.; Robertson, J. *Phys. Rev. B* **2000**, *61*, 14095−14107.
(38) Ferrari, A. C.; Robertson, J. *Philos. Trans. R. Soc. London, Ser. A* **2004**, *362*, 2477−2512.
(39) Xu, J. S.; Chen, Q. Y.; Swain, G. M. *Anal. Chem.* **1998**, *70*, 3146−3154.
(40) Swain, G. M. *J. Electrochem. Soc.* **1994**, *141*, 3382−93.
(41) Kneten, K. R.; McCreery, R. L. *Anal. Chem.* **1992**, *64*, 2518−24.
(42) Chen, P.; McCreery, R. L. *Anal. Chem.* **1996**, *68*, 3958−3965.
(43) Bennett, J. A.; Wang, J.; Show, Y.; Swain, G. M. *J. Electrochem. Soc.* **2004**, *151*, E306−E313.
(44) Wang, S.; Swope, V. M.; Butler, J. E.; Feygelson, T.; Swain, G. M. *Diamond Relat. Mater.* **2009**, *18*, 669−677.
(45) Fischer, A. E.; Show, Y.; Swain, G. M. *Anal. Chem.* **2004**, *76*, 2553−2560.
(46) Kim, D. Y.; Wang, J.; Yang, J.; Kim, H. W.; Swain, G. M. *J. Phys. Chem. C* **2011**, *115*, 10026.
(47) Bowling, R.; Packard, R. T.; McCreery, R. L. *Langmuir* **1989**, *5*, 683.
(48) Poon, M.; McCreery, R. L. *Anal. Chem.* **1988**, *58*, 2745.
(49) Jia, J.; Kato, D.; Kurita, R.; Sato, Y.; Maruyama, K.; Suzuki, K.; Hirono, S.; Ando, T.; Niwa, O. *Anal. Chem.* **2007**, *79*, 98−105.
(50) Niwa, O.; Jia, J.; Sato, Y.; Kato, D.; Kurita, R.; Maruyama, K.; Suzuki, K.; Hirono, S. *J. Am. Chem. Soc.* **2006**, *128*, 7144−7145.
(51) Sekioka, N.; Kato, D.; Ueda, A.; Kamata, T.; Kurita, R.; Umemura, S.; Hirono, S.; Niwa, O. *Carbon* **2008**, *46*, 1918−1926.
(52) Kato, D.; Sekioka, N.; Ueda, A.; Kurita, R.; Hirono, S.; Suzuki, K.; Niwa, O. *J. Am. Chem. Soc.* **2008**, *130*, 3716−3717.